Article:

Cepero-Mejıas, F., Phadnis, V.A., Kerrigan, K. orcid.org/0000-0001-6048-9408 et al. (1 more author) (2021) A finite element assessment of chip formation mechanisms in the machining of CFRP laminates with different fibre orientations. Composite Structures, 268. 113966. ISSN 0263-8223

https://doi.org/10.1016/j.compstruct.2021.113966

A finite element assessment of chip formation mechanisms in machining of CFRP laminates with different fibre orientations

Cepero-Mejías F.[a,b,c,*], Curiel-Sosa J. L.[b,c], Kerrigan K.[d], Phadnis V. A.[e]

[a]*Industrial Doctorate Centre in Machining Science, The University of Sheffield, Sir Frederick Mappin Building, Mappin Street, S1 3JD Sheffield, United Kingdom.*
[b]*Computer-Aided Aerospace & Mechanical Engineering (CA2M) Research Group, Sir Frederick Mappin Building, Mappin Street, S1 3JD Sheffield, United Kingdom.*
[c]*Department of Mechanical Engineering, The University of Sheffield, Sir Frederick Mappin Building, Mappin Street, S1 3JD Sheffield, United Kingdom.*
[d]*Advanced Manufacturing Research Centre with Boeing, University of Sheffield, Advanced Manufacturing Park, Wallis Way, Catcliff, Rotherham, S60 5TZ, United Kingdom.*
[e]*3M UK Plc, Bracknell RG12 8HT, United Kingdom.*

Abstract

The virtual assessment of a composite machining process using finite element (FE) models constitute a cost-effective solution to study the shape quality of a machined part. Thus, the correct simulation of the chip fracture becomes essential to obtain consistent numerical results. This work develops an original FE approach to emulate the chip formation in the machining of carbon fibre reinforced polymer (CFRP) laminates. Material removal is conducted using a combination of Puck's and Hashin's composite failure criteria to assess the onset of composite damage modes. Subsequently, mechanical properties of the damaged elements are linearly degraded increasing remarkably the element strain values along this phase. Finally, a novel strain-based element deletion criterion developed in this research is applied to reliably simulate the chip release process. Five different cutting configurations are successfully modelled in this research observing the influence of relevant fibre orientation and cutter rake angles on chip formation. The shape of the simulated chips reaches a high similarity with the chips obtained in relevant experimental trials collected from the literature. Useful insights about the modelling of sub-surface damage in composite machining are also collated in this investigation. For instance, the modelling of the fibre bending damage which take place in the machining of 90° laminates is analysed in detail.

Keywords: Machining, Chip formation, Finite element, Modelling, Orthogonal cutting, Composite

*Corresponding author.
Email addresses: fmcepero1@sheffield.ac.uk (Cepero-Mejías F.), j.curiel-sosa@sheffield.ac.uk (Curiel-Sosa J. L.), k.kerrigan@sheffield.ac.uk (Kerrigan K.), ved.phadnis@gmail.com (Phadnis V. A.)

1. Introduction

In the last decades, the use of composite materials has been steadily increased in high-performance applications [1, 2]. This is motivated due to the tailored properties achieve excellent structural performance in the directions more loaded with a notable weight reduction. Because of this reason, composites are especially used in the aerospace industry, where aircraft models such as the Boeing 787 have achieved a total weight fraction in composites of a 50% [3]. Additionally, the use of these components will allow a substantial growth of the aerostructure capabilities on the oncoming years. For instance, the Aerospace Technology Institute (ATI) expect a reduction of a 50% and 35% in the buy-to-fly ratio and airframe weight, respectively and an increment of a 40% in productivity rates by 2035 [4].

Composite parts they are often need to be machined to accomplish the strict requirements demanded in high-tech applications. However, composites are considered materials hard to machine because the presence of abrasive fibre or low thermal conductivity resins induced a rapid tool wear. Rounded cutter edges tend to bend fibres instead of shearing them away inducing the presence of a crack in the underlying machined surface [5]. Another important type of damage to consider in composite machining is the inter-ply delamination. This defect is mainly caused by drilling operations due to the high thrust applied by the drill bit on the laminate. In general, low cutting velocities and high feed rates are demonstrated to increase substantially the extension of the delamination in the outer plies [7]. Considering that these aforementioned defects considerably reduce the strength or fatigue life of laminates [8], the investigation to mitigate these severe machining induced damages is essential to guarantee the structural integrity of composite parts.

In general terms, the experimental investigation of optimum composite machining parameters of high-quality parts present several problems. The high cost of composite materials together with factors such as the low repeatability in tests, the low automation level in the manufacturing process or the difficult calibration and high cost of the measurement equipment employed make the experimental research an expensive and laborious process. Because of this, the use of other non-destructive and feasible alternatives are recommended. Finite element method offers a cost-effective virtual tool to investigate in detail the key points of a machining process. Several characteristic failures in composite machining such as inter-ply delamination [9, 10] or fibre and matrix damage modes [11] can be successfully addressed using this approach. Additionally, cutting parameters such as feed rate, cutter morphology or fibre orientation among others might be numerically analysed to optimise the machining process without a significant increment of the cost and time. For these reasons, the development of robust FE investigations in this research field has gained great value these days.

To date, most FE studies have investigated the influence of cutting parameters on machining forces and machining induced damage in composite machining. Santiuste et al. [12] proved that sub-surface damage is much more severe in GFRP with a ductile chip fracture than in CFRP laminates that experience a brittle behaviour. Soldani et al. [13] investigated the influence tool wear on machining, concluding that the machining with sharp tool edge radius is essential to obtain low induced damages. Zenia et al. [14] studied the influence of cutting parameters on machining responses. Increments in the depth of cut are found to raise machining forces and induced damage, while changes in the rake angle are not observed to be relevant in the machining responses. Wang et al. [15] assessed the influence of the fibre orientation on the machining induced damage. Because of the fibre bending phenomenon 90° laminates are found to be the ones with higher damage penetration. Finally, Cepero-Mejias et al. [16] introduced the spring-back phenomenon in his simulations to improve the accuracy of the predictions. It was concluded that the use of high release angles conducts to decrease sub-surface damage.

A critical review of the state-of-art revealed that despite chip fracture is intimately connected with the prediction of machining responses; it has not been widely modelled up to date [17]. Most relevant publications are summarised in the following lines. Lasri et al. [18] modelled the chip fracture in laminates from 15° to 90° with the use of three composite failure criteria. This study concluded that chip fracture takes place in the fibre/matrix interface, so the lower the fibre orientation is, the larger the chip length is obtained. More recently, Cepero-Mejas et al. [19] simulated the chip fracture of a laminate with high accuracy. This was achieved with the development of a novel study in composite machining based on the use of a linear continuum damage mechanics (CDM) approach together with a strain-based element deletion algorithm in composite machining. However, all the investigations mentioned above have several limitations because they are developed in simplified 2D FE models and not all fibre orientations are successfully simulated. 2D FE model are limited to the study of orthogonal cutting operations because it does not take into account the out-of-plane effect of the process; thus excluding more complex machining operations such as drilling, milling or turning. The study of these machining processes is of great interest to the industry and can only be addressed using 3D finite element models. Therefore, the development of more complex 3D FE models is required to enhance the quality of the machining responses predictions in the oncoming investigations.

This manuscript develops an original methodology to model in 3D FE models the chip fracture in a composite orthogonal cutting process with several fibre orientations. The paper layout is broken as follows. Section 2 provides a description of more important numerical aspects accounted for in this work. Details of the linear energy-based composite damage model employ in this investigation are given in section 3. A thorough discussion of the particularities modelled at each fibre orientation simulated is encountered in section 4. Finally, section 5 offers a general view of this research remarking the most relevant findings extracted from this numerical assessment.

2. FE Model characteristics

This section aims to clarify the most relevant aspects of the 3D FE model developed in this research. This information is collected in two separate sections where numerical details regarding mesh distribution, geometry, material and friction model employed are described.

2.1. General model features

A representative portion of the laminate of 1 mm height, 2 mm long and 50 μm width is assessed in this work, see Fig. 1(a). The height and longitudinal dimensions of the model allow to recreate the chip release without the interaction of the imposed boundary conditions at the edges. A small thickness of 50 μm is selected to reach a reasonable computational times because the out-of-plane effect is negligible in the developed simulations. The cutting tool is positioned in the middle of the laminate to accurately emulate cutting conditions when the tool moves along the edge of the laminate. Additionally, two separate boundary conditions are implemented to mimic a clamped laminate: horizontal displacement of laminate is restricted in lateral sides, while bottom surface of the laminate fully fixed as shown in Fig. 1(b). The cutting parameters modelled in this investigation, which are visualised in Fig. 1(b). are collected in Table 1.

Table 1
Cutting variables employed in this work

Rake angle (α)	Relief angle (β)	Tool edge radius	Depth of cut	Cutting speed
10 °	10 °	10 μm	200 μm	100 mm/s

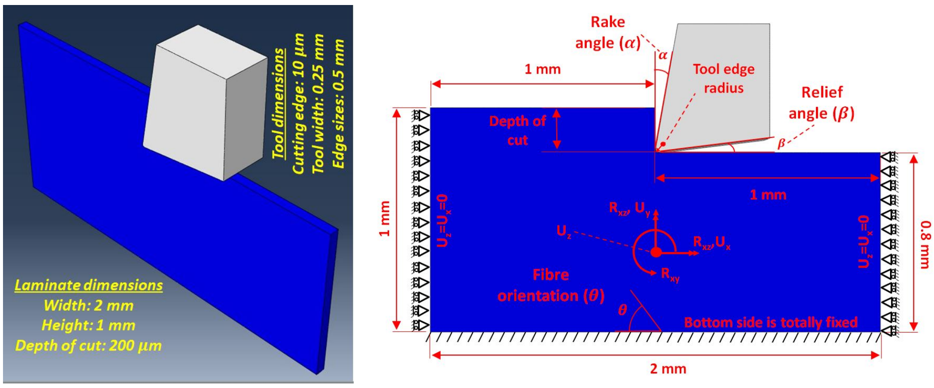

(a) (b)

Fig. 1. Representation of the FE model simulated: (a) 3D perspective view (b) Boundary conditions and relevant cutting parameters modelled

Four fibre orientations are simulated in this research to assess several possible scenarios in composite machining: 0°, 45°, 90° and 135°. The mechanical properties of the CFRP laminate modelled in this research are listed in Tables 2 and 3, respectively. To reduce the computational cost, the cutting tool is assumed to be rigid, i.e. elastic stiffness of the cutting tool considered to be remarkably higher than the CFRP laminate. This approach is considered to be valid for two reasons: firstly, magnitudes of cutting process parameters (especially depth-of-cut and cutting speed as these govern the cutter-workpiece contact area at any given instance) in this study are not large enough to cause a noticeable deformation to the cutter. Secondly, modelling of tool wear is out-of-scope of the current study, this will be a matter of future consideration.

Table 2
Elastic properties of the CFRP laminate

$E_{11}(GPa)$	$E_{22} = E_{33}(GPa)$	$G_{12} = G_{13} = G_{23}(GPa)$	$\upsilon_{12} = \upsilon_{13}$	υ_{23}
136.6	9.6	5.2	0.29	0.4

Table 3
Strength properties of the CFRP laminate

$X_T(MPa)$	$X_C(MPa)$	$Y_T = Z_T(MPa)$	$Y_C = Z_C(MPa)$	$S_{12} = S_{13} = S_{23}(MPa)$
2720	1690	111	214	115

2.2. Mesh and friction model performed

Hexagonal C3D8R meshed elements available in Abaqus/Explicit are used in this investigation. A thorough distribution of the element sizes is meshed to guarantee the accuracy of the results in a reasonable computational time.

In the cutting tool, the elements are refined around the cutting edge to recreate the cutting edge morphology accurately with element sizes of 2 μm, while for the rest of the cutting tool they are around 10 μm. Three types of mesh regions are distinguished in the composite laminate: one refined mesh, two intermediate meshes and one coarse mesh. The refined mesh is allocated in the cutting area in front of the tool with an element size 5 μm. Both intermediate meshes increase gradually one dimension of the element size from 5 μm to 100 μm, while the coarse mesh element sizes are steadily incremented from 5 μm to 100 μm, refer to Fig. 2(a).

Along the tool width, only five partitions are modelled to reduce the number of meshed elements and reduce the computational cost of the model. In the case of the composite laminate, ten partitions are carried out to have elements in the cutting region with an aspect ratio of 1, as shown in Fig. 2(b). This aspect ratio is used to notably enhance the accuracy of the numerical results **??**.

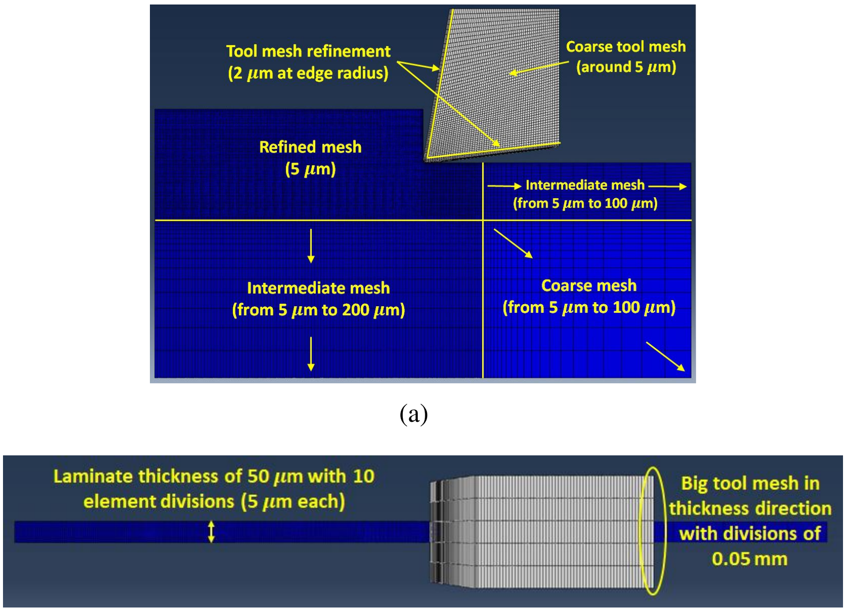

(a)

(b)

Fig. 2. Representation of meshed areas of the model: (a) Laminate and tool mesh distribution (b) Mesh distribution in the thickness

A constant coulomb friction coefficient of 0.1 is employed to simulate the laminate/tool contact.

This coefficient is selected because several investigations concluded that the friction coefficients between CFRP laminates and PCD tools are close to this magnitude [20, 21].

3. FEM damage algorithm basics

The proposed damage model used here is implemented in Abaqus/Explicit via an user-defined Fortran VUMAT subroutine. Six different damage modes are studied in this model: two for fibres (d_{ft} *and* d_{fc}), other two for matrix dominated damage in the laminate plane (d_{mt2} *and* d_{mc2}) and rest two for matrix dominated damage in the thickness direction (d_{mt3} *and* d_{mc3}). All these damage modes are combined in the compliance matrix as follows.

$$\left[S_{ij}\right] = \begin{bmatrix} \frac{1}{(1-d_f)E_{11}} & -\frac{\nu_{12}}{E_{11}} & -\frac{\nu_{13}}{E_{11}} & 0 & 0 & 0 \\ -\frac{\nu_{21}}{E_{22}} & \frac{1}{(1-d_m)E_{22}} & -\frac{\nu_{23}}{E_{22}} & 0 & 0 & 0 \\ -\frac{\nu_{31}}{E_{33}} & \frac{1}{(1-d_m)E_{33}} & -\frac{\nu_{23}}{E_{33}} & 0 & 0 & 0 \\ 0 & 0 & 0 & \frac{1}{(1-d_{s1})G_{12}} & 0 & 0 \\ 0 & 0 & 0 & 0 & \frac{1}{(1-d_{s2})G_{13}} & 0 \\ 0 & 0 & 0 & 0 & 0 & \frac{1}{(1-d_{s3})G_{23}} \end{bmatrix} \tag{1}$$

$$Here,\ d_{s1} = 1-(1-d_{ft})(1-d_{fc})(1-d_{mt2})(1-d_{mc2})\ ; d_{s2} = 1-(1-d_{ft})(1-d_{fc})(1-d_{mt3})(1-d_{mc3})$$

$$d_{s3} = 1-(1-d_{mt2})(1-d_{mc2})(1-d_{mt3})(1-d_{mc3})$$

$$d_f = max\{d_{ft}, d_{fc}\}\ ;\ d_{m2} = max\{d_{mt2}, d_{mc2}\}\ ;\ d_{m3} = max\{d_{mt3}, d_{mc3}\}$$

$$d_I \epsilon [0,1]\ and\ I = (ft, fc, mt2, mc2, mt3, mc3)$$

However, in Abaqus, the constitutive behaviour of the material is defined with the elastic stiffness matrix. The components of the stiffness matrix employed in this research are illustrated below.

$$\begin{aligned} C_{11} &= E_{11}(1-d_f)\left[1-(1-d_{m2})(1-d_{m3})\nu_{23}^2\right]/A \\ C_{12} &= E_{22}(1-d_f)(1-d_{m2})\left[(1-d_{m3})\nu_{13}\nu_{23}+\nu_{12}\right]/A \\ C_{22} &= E_{22}(1-d_{m2})\left[1-(1-d_f)(1-d_{m3})\nu_{13}\nu_{13}\right]/A \\ C_{13} &= E_{33}(1-d_f)(1-d_{m3})\left[(1-d_{m2})\nu_{12}\nu_{23}+\nu_{13}\right]/A \\ C_{33} &= E_{33}(1-d_{m3})\left[1-(1-d_f)(1-d_{m2})\nu_{12}\nu_{21}\right]/A \\ C_{23} &= E_{33}(1-d_{m2})(1-d_{m3})\left[(1-d_f)\nu_{12}\nu_{31}+\nu_{23}\right]/A \\ C_{44} &= G_{12}(1-d_f)(1-d_{m2}) \\ C_{55} &= G_{13}(1-d_f)(1-d_{m3}) \\ C_{66} &= G_{23}(1-d_{m2})(1-d_{m3}) \end{aligned} \tag{2}$$

$$with\quad A = 1-(1-d_f)(1-d_{m2})\nu 12\nu_{21}-(1-d_{m2})(1-d_{m3})\nu_{23}^2-(1-d_f)(1-d_{m3})\nu_{13}\nu_{31}$$

$$-2(1-d_f)(1-d_{m2})(1-d_{m3})\nu_{12}\nu_{31}\nu_{23}$$

Damage initiation is assessed using Hashin's failure criterion [22] for fibre damage modes, refer to Eqs. (3) and (4). This criterion is commonly used in composite machining because its simplicity and high capabilities to predict accurate results [23]. Damage initiation occurs when a damage activation function F_I reaches a value ≥1, as explained below.

- Fibre traction ($\sigma_{11} \geq 0$)

$$F_{ft} = \left(\frac{\sigma_{11}}{X_T}\right)^2 + \left(\frac{\sigma_{12}}{S_{12}}\right)^2 + \left(\frac{\sigma_{13}}{S_{13}}\right)^2 \geq 1 \tag{3}$$

- Fibre compression ($\sigma_{11} < 0$)

$$F_{fc} = \left| \frac{\sigma_{11}}{X_C} \right| \geq 1 \tag{4}$$

In case of the matrix damage modes, Puck's plane stress failure criterion [24] is selected because of its excellent capabilities to accurately simulate composite failure in off-axis loading scenarios [25]. Puck's failure criteria consider three separate damage modes: Mode A, Mode B and Mode C. Mode A occurs when the transverse stresses are positive, while Mode B and Mode C predict the matrix fracture under compression loading. Therefore, in this work, the matrix compression damage is initialised when Mode B or Mode C criteria is achieved. The expressions representing these damage modes are as follows.

- Matrix Mode A ($\sigma_{22} \geq 0$)

$$F_{mma} = \sqrt{\left(\frac{\sigma_{12}}{R^A_{\perp\|}}\right)^2 + \left(1 - \frac{p^{(+)}_{\perp\|}}{R^A_{\perp\|}} R^{(+)A}_{\perp}\right)^2 \left(\frac{\sigma_{22}}{R^{(+)A}_{\perp}}\right)^2} + \frac{p^{(+)}_{\perp\|}}{R^A_{\perp\|}}\sigma_{22} \geq 1 \tag{5}$$

- Matrix Mode B ($\sigma_{22} < 0$ *and* $\sigma_{22} > -R^A_{\perp\perp}$)

$$F_{mmb} = \sqrt{\left(\frac{\sigma_{12}}{R^A_{\perp\|}}\right)^2 + \left(\frac{p}{R}\right)^2 \sigma_{22}^2} + \left(\frac{p}{R}\right)\sigma_{22} \geq 1 \tag{6}$$

- Matrix Mode C ($\sigma_{22} \leq -R^A_{\perp\perp}$)

$$F_{mmc} = \frac{1}{2\left[1 + \left(\frac{p}{R}\right) R^A_{\perp\perp}\right]} \left[\left(\frac{\sigma_{12}}{R^A_{\perp\|}}\right)^2 + \left(\frac{\sigma_{22}}{R^A_{\perp\perp}}\right)^2\right] \frac{R^A_{\perp\perp}}{-\sigma_{22}} \geq 1 \tag{7}$$

Note that, in the above, the typical nomenclature used by Puck to define his model is employed. For brevity purpose, the meaning of these variables are not specified in this paper. Interested readers to achieve a better understanding of Puck's failure criteria are referred to go to **Reference [24]**.

Once damage onset is achieved, a linear energy-based mechanical properties degradation law is applied. Damage variables increase from 0 to 1 in the range of equivalent displacements between initial and final equivalent displacements calculated in Eqs. (8) and (9), respectively. The expression used to calculate the damage modes magnitude is shown in Eq. (10).

$$\delta^0_{I,eq} = \frac{\delta_{I,eq}}{F_I} \tag{8}$$

$$\delta^f_{I,eq} = \frac{2G^c_I F_I}{\sigma_{I,eq}} \tag{9}$$

$$d_I = \frac{\delta^f_{I,eq}\left(\delta_{I,eq} - \delta^0_{I,eq}\right)}{\delta_{I,eq}\left(\delta^f_{I,eq} - \delta^0_{I,eq}\right)} \quad (d_I \in [0,1]\ and\ I = (ft, fc, mt, mc)) \tag{10}$$

Here, the term F_I represents the damage activation function value when a failure mode takes place. $\sigma_{I,eq}$ denote the equivalent stress of a failure mode. Finally, $\delta_{I,eq}$ is the equivalent displacement calculated after damage happens. These variables are defined in this paper following the same methodology previously used by Goundong *et al.* [26] to degrade the properties of a braided composite. Finally, the critical fracture toughness values (G^C_I) used in this investigation are shown in Table 4.

Table 4
Critical fracture toughness employed in this work

N/mm	G^c_{ft}	G^c_{fc}	G^c_{mt}	G^c_{mc}
G^C_I	100	100	1	1

A maximum damage of 0.99 is allowed for matrix damage modes and 0.999 for the fibre damage modes. These maximum values are chosen to avoid the problems given by element with an excessive deformation [18]. The mechanical properties degradation lead to rapid increments in the deformation of the damaged meshed elements that are eroded after achieving a maximum value to emulate the chip formation process. The maximum strain criteria chosen in this research is different for every case studied to mimic the particularities of every machining configuration. These criteria are explained in detail in the following section.

4. Numerical chip formation assessment

Five chip fracture scenarios are successfully assessed with the deletion of the element which overcomes determine strain limits. Firstly, the experimental basics of the machining cases analysed in this manuscript which are studied by other researchers are explained. Subsequently, the modelling of the chip fracture scenarios investigated are explained; these simulations are in the right balance with experimental findings previously defined. Numerical details and particularities employed in every studied case are also provided. Finally, the overall strain-based element deletion criteria implemented to simulate successfully all the studied cases is explained.

4.1. Experimental insights in the chip formation of composite machining

In composite machining, the main factor which controls the chip fracture process is the fibre orientation. In this investigation, cutting tools with positive rake angles are selected as a reference. Four distinct chip classifications according to the fibre orientation in the composite machining with positive rake angles (superior to 0°) can be distinguished: (1) 0°, (2) positive fibre orientations (0° $< \theta <$ 90°), (3) 90° and (4) negative fibre orientations ($\theta >$ 90°). Additionally, the particular micro-buckling of the fibres observed in the machining using cutting tools with 0° rake angle is modelled in this research.

In the following lines, a brief description of the particularities of every chip formation mechanism aforementioned is provided. Interested readers to know more detailed information about this topic are referred to [15, 27, 28]. All these cases are visualised in Fig. 3.

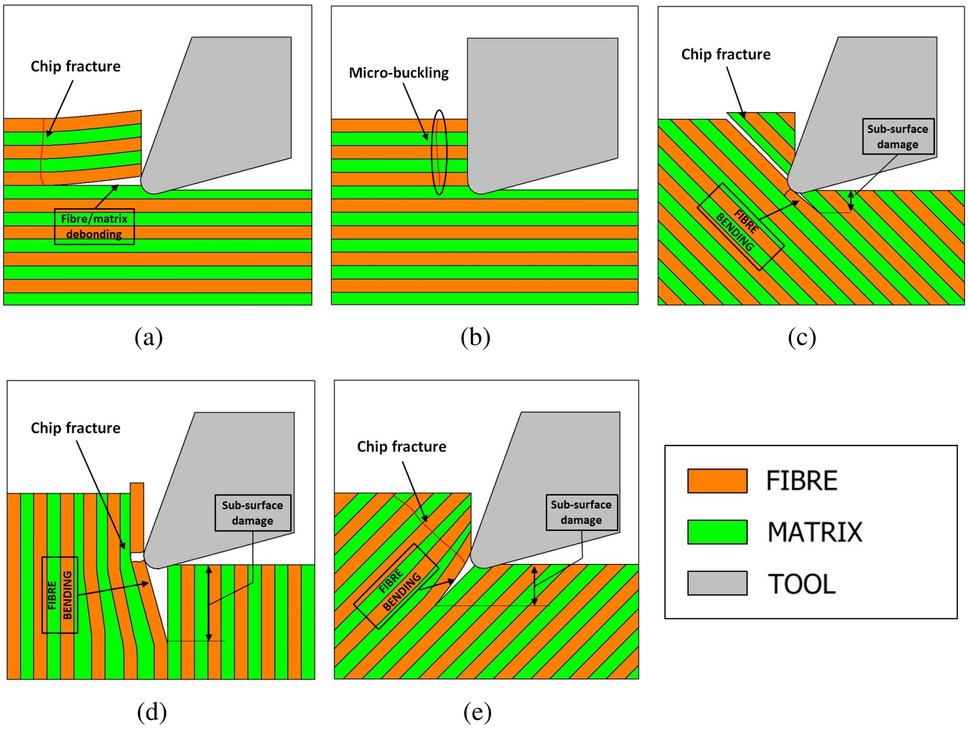

Fig. 3. Representation of the different chip fracture scenarios studied in this research: (a) Fibre orientation of 0°, (b) Fibre orientation of 0° with a rake angle of 0°, (c) Fibre orientation of 0° with a rake angle of 0°, (d) Fibre orientation of 90° and (e) Negative fibre orientations or superior to 90°

- **Fibre orientation of 0°**: firstly, a mode I fracture parallel to the fibre peel the laminate from the tool edge radius, creating a separate layer which slides over the rake face. This fracture occurs because the tensile strength of the matrix is much lower than the strength of the fibre under compression loadings. Secondly, the cutter advance induce a notable increase in the bending moment of the separate layer. Finally, the chip breaks perpendicularly to the fibre direction because the fibre bending strength is exceeded, as shown in Fig. 3(a).

- **Fibre orientation of 0° with 0° rake angle**: the high fibre compression occasioned by the rigid tool/workpiece contact originate the micro-buckling of the fibres with a small chip length. This mechanism is visualised in Fig. 3(b).

- **Positive fibre orientations** $0° < \theta < 90°$: the chip slides parallel to the fibre orientation in a mode II fracture because produced by the high compressive forces induced with the advancement of the cutting tool, as represented in Fig. 3(c).

- **Fibre orientation of 90°**: small fragments of fibre and matrix are sheared away parallel to the fibre orientation. The fibre is cut in this configuration because of the high compression of the shear forces that take place in the fibre area in contact with the tool edge radius. This contact produces a high bending moment in the fibre, which induce a mode I fracture obtaining substantial sub-surface damage [15], refer to Fig. 3(d).

- **Negative fibre orientations** $\theta > 90°$: the chip is removed with a mode II fracture perpendicular of the fibre because of the bending of fibre induced by severe compressive forces produced by the cutting tool. As a consequence of the fibre bending moment generated with the contact of the tool, significant underlying machining damage is induced in the laminate, as represented in Fig. 3(e).

4.2. Numerical assessment

Details about the modelling of the machining configurations described in the previous section are provided here. For this purpose, five different simulations are performed with the following fibre orientations: (1) 0°, (2) 0° and rake angle of 0°, (3) 45°, (4) 90° and (5) 135°. Particularities and numerical methodologies implemented in the simulation of every studied case are exposed below.

4.2.1. Fibre orientation of 0°

Although chip formation in this machining configuration consists of two phases: composite layer debonding and vertical fracture of the fibres, the simulation of the vertical fracture of the fibres is not modelled here. To simulate this feature, the length of the laminate in front of the cutting tool should be increased to generate the required bending moment to break the fibres. In addition, it is necessary to simulate a thickness superior to the depth of cut to drive the chip upwards within the cutting plane and not in the thickness direction as it would be done in the current model. These changes would exponentially increase the computational cost of the model; thus, the simulation of this feature is decided to be addressed in further investigations. The perspective and front views of the composite layer debonding simulated are presented in Fig. 4.

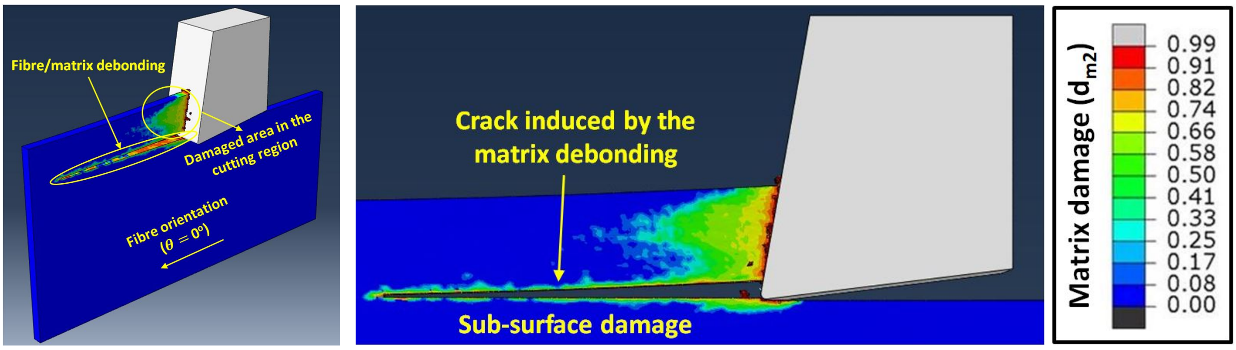

(a) (b)

Fig. 4. Representation of the FE model simulated with a fibre orientation of 0°: (a) 3D perspective view (b) Front view

The composite layer debonding occurs in regions with high transversal strains to the fibre direction and a substantial matrix traction damage. Therefore, to simulate this feature the meshed elements with high transversal strain (ε_{22}) need to be deleted. In this work, the erosion of the element is imposed when it reaches a value of $\varepsilon_{22} \geq 0.15$. As a result, the expected debonding is obtained using this methodology observing high matrix traction damage ($d_{mt2} \epsilon [0.9 - 0.99]$) in the deleted elements. These statements are visualised in Fig. 5 which represents the evolution of ε_{22} and d_{mt2} along the simulation time of a representative meshed element which is deleted during the simulation to generate the layer debonding.

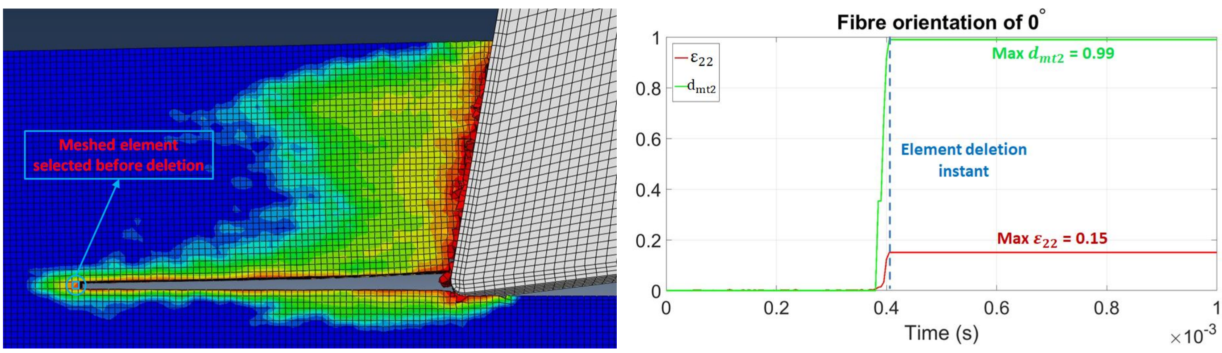

(a) (b)

Fig. 5. Representation of a representative meshed element deleted to simulate the chip of a laminate with a fibre orientation of 0°: (a) Meshed element selected before deletion (b) Evolution of d_{mt2} and ε_{22} during the simulation time.

4.2.2. Fibre orientation of 0° with 0° rake angle

In this simulation, the fibre micro-buckling that take place close to the cutting tool is accurately simulated. A significant large damaged area in front of the cutting tool is obtained due to the abrupt contact of the rake face with the laminate simultaneously and the fibre micro-buckling represent an aggressive fracture. Both statements mentioned above are visualised in Fig. 6.

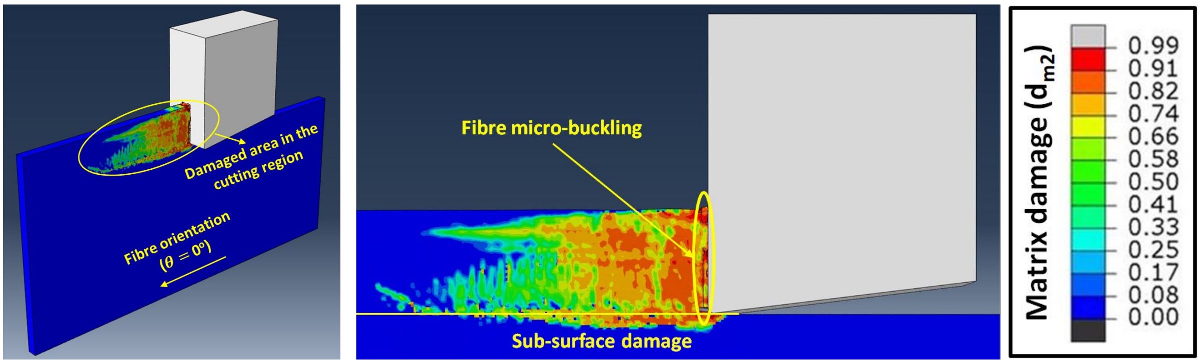

(a) (b)

Fig. 6. Representation of the FE model simulated with a fibre orientation of 0° and a rake angle of 0°: (a) 3D perspective view (b) Front view

This fibre micro-buckling occurs after the mechanical properties in the fibre direction are severely reduced with a high fibre compression damage ($d_{fc} \geq 0.9$). Therefore, for emulating this fracture behaviour, the deletion of elements with high fibre compression strain values of $-\varepsilon_{11} \geq 0.2$ is selected. These previous arguments are represented with the evolution of the variables $-\varepsilon_{11}$ and d_{fc} of one deleted element during the simulation time in Fig. 7

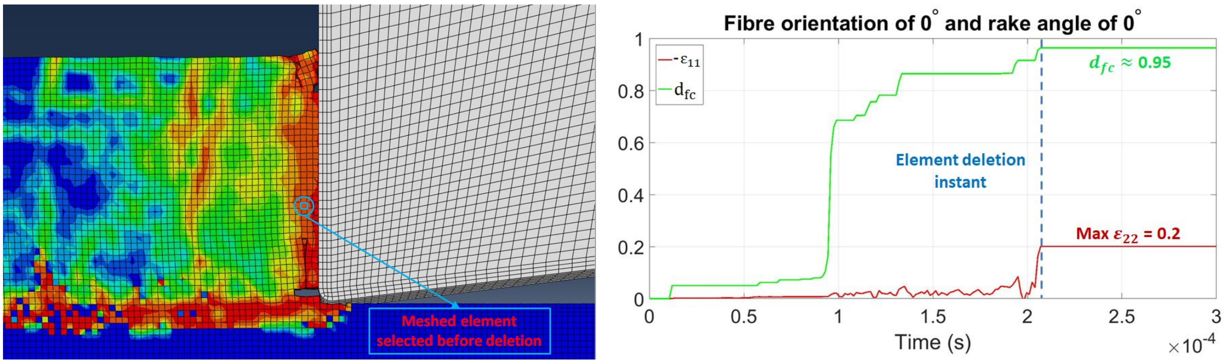

(a) (b)

Fig. 7. Representation of a representative meshed element deleted to simulate the chip of a laminate with a fibre orientation of 0° and a rake angle of 0°: (a) Meshed element selected before deletion (b) Evolution of d_{fc} and ε_{11} during the simulation time.

4.2.3. Fibre orientation of 45°

A chip release fracture plane of 43° is achieved, as shown in Fig. 8(b). This fracture is produced because the deletion of elements is mainly occasioned by shear stresses which delete the elements mainly in the diagonal direction. However, occasionally they are deleted in horizontal inserting this small deviation of 2° with respect to the fibre orientation during the crack growth due to the numerical errors in the damage transmission using this methodology to recreate the crack. A parallel alignment with the fibre orientation of the mesh might mitigate this defect. Finally, underlying the machined surface, it is appreciated that the damage distribution is parallel to the fibre as it occurs in reality (refer to Fig. 3(c)), see Fig. 8

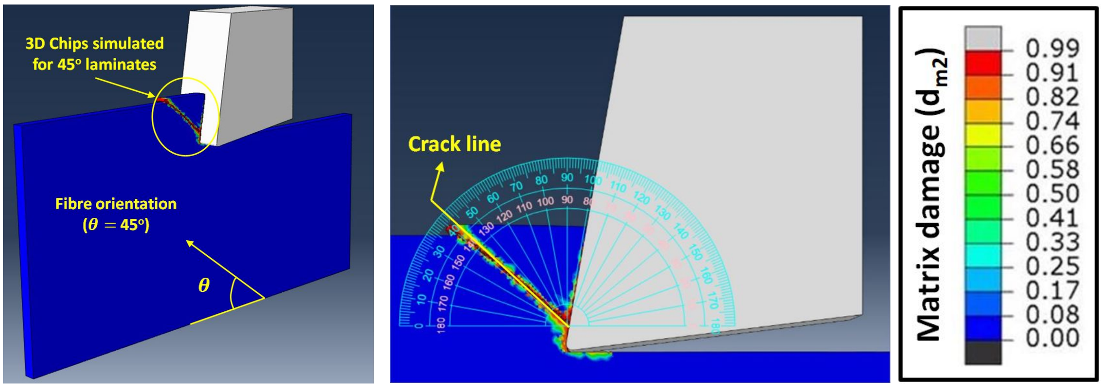

(a) (b)

Fig. 8. Representation of the FE model simulated with a fibre orientation of 45°: (a) 3D perspective view (b) Front view

The chip fracture is generated because of the high shear stresses produced in the region where the chip slides out. Therefore, the deletion of element with a high in-ply shear strains (ε_{12}) values of $\varepsilon_{12} \geq 0.325$. This statement is visualised in the evolution of ε_{12} of a representative deleted element eroded during the simulation in Fig. 9. In this case, both matrix and fibre damages could be high (0.9 or superior) in the chip release region, because shear stresses activate simultaneously both damage types. To support this argument, in Fig. 9(b) is represented the evolution of the d_{m2}. It is observed that this damage assessed achieves values higher than 0.9 before the final deletion.

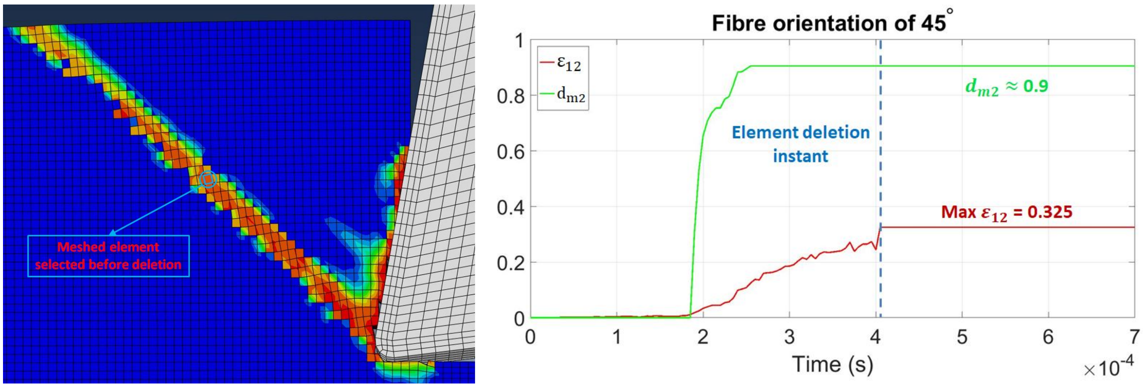

(a) (b)

Fig. 9. Representation of a representative meshed element deleted to simulate the chip of laminates with a fibre orientation of 45°: (a) Meshed element selected before deletion (b) Evolution of d_{m2} and ε_{12} during the simulation time.

4.2.4. *Fibre orientation of 90°*

Two laminate fractures are modelled here: (1) small chip fragments in front of the tool and (2) fibre bending damage below the tool. The small chip fragments are simulated due to the high compression stresses produced because of the advance of the cutting tool, while the fibre bending damage is originated because of the high matrix traction damage (d_{m2}). Both fractures are clearly visualised in Fig. 10.

Two separate considerations in the deletion of elements are taken to simulate both fracture modes. A high compression value in the transversal compressive strains of $-\varepsilon_{22} \geq 1.2$ is selected to simulate the small chip fragments in front of the cutting tool. In the case of fibre bending damage, transverse tensile strain values of $\varepsilon_{22} \geq 0.2$ are used. The representation of the evolution of the previous commented strain values for both studied fractures is represented in Fig. 11.

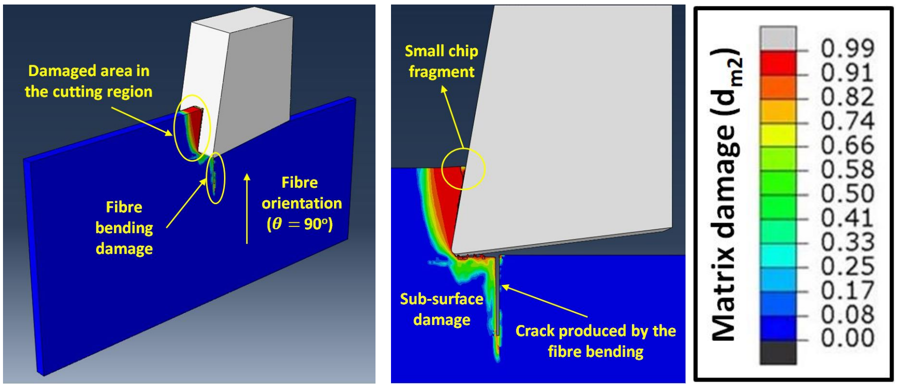

(a) (b)

Fig. 10. Representation of the FE model simulated with a fibre orientation of 90°: (a) 3D perspective view (b) Front view

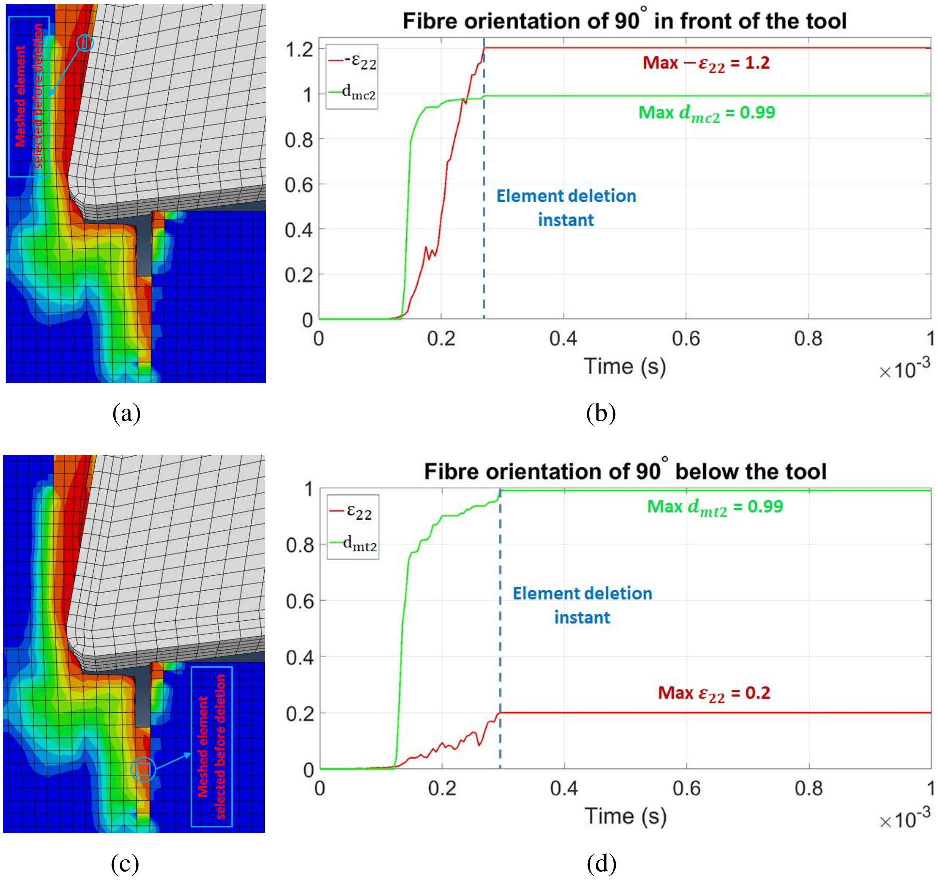

(a) (b) (c) (d)

Fig. 11. Representation of a representative meshed element deleted to simulate the chip of laminates with a fibre orientation of 90°: (a) Meshed element selected in front of the cutting tool before deletion, (b) Evolution of d_{mc2} and ε_{22} during the simulation time, (c) Meshed element selected below of the cutting tool before deletion, (d) Evolution of d_{mt2} and ε_{22} during the simulation time.

4.2.5. Fibre orientation of 135°

A precise fracture perpendicular to the fibre direction is achieved in this simulation, as shown in Fig. 12(b). This fracture is motivated for the high shear stresses observed in the fracture zone. Furthermore, it is appreciated that the damage underlying the machined surface is parallel to the fibre direction as it is explained in the previous subsection of this manuscript, see Fig. 12.

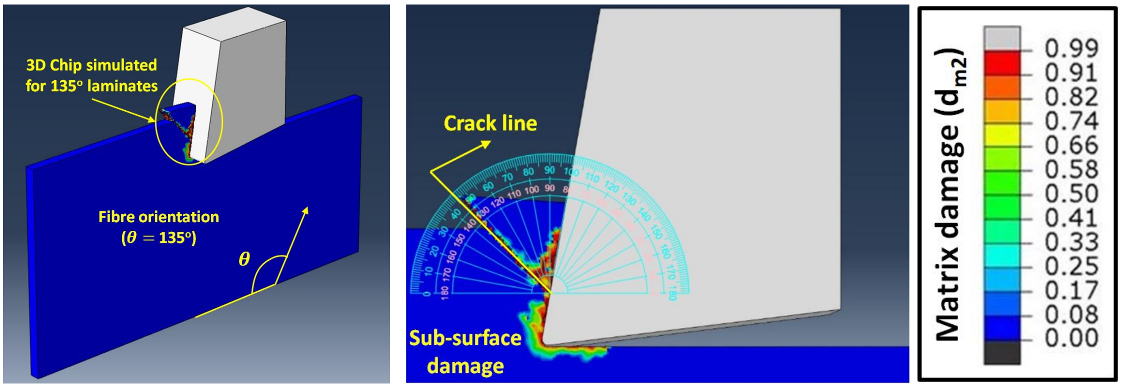

(a) (b)

Fig. 12. Representation of the FE model simulated with a fibre orientation of 135°: (a) 3D perspective view (b) Front view

In order to predict the fibre breakage, the fibre compression equation from Hashin's composite failure criteria exposed in Eq. (4) is modified to take into account the shear effects. A factor of 0.8 is incorporated to address this matter leading to the final quadratic expression represented in Eq. (11). Expected results are reached as it is illustrated in Fig. 13, which illustrates the fibre compression damage (d_{fc}) is propagated through the laminate perpendicularly to the fibre direction.

- Fibre compression ($\sigma_{11} < 0$)

$$F_{ft} = \left(\frac{\sigma_{11}}{X_T}\right)^2 + 0.8\left(\frac{\sigma_{12}}{S_{12}}\right)^2 + 0.8\left(\frac{\sigma_{13}}{S_{13}}\right)^2 \geq 1 \tag{11}$$

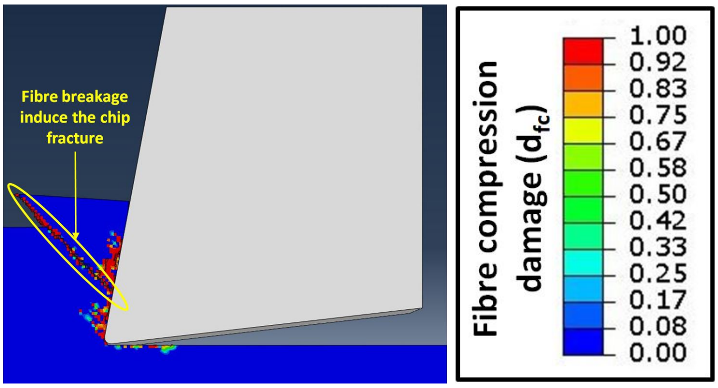

Fig. 13. Illustration of the fibre compression damage previous to the chip release in laminates with a fibre orientation of 135°.

The same strategy of element deletion taken in the chip formation of laminate with a fibre orientation of 45° is used here. Meshed elements are deleted when they achieve a shear strain levels of $\varepsilon_{12} \geq 0.325$. In this particular case, the fibre compression damage is the highest in the deleted elements achieving values close to 1, as appreciated in Fig. 14.

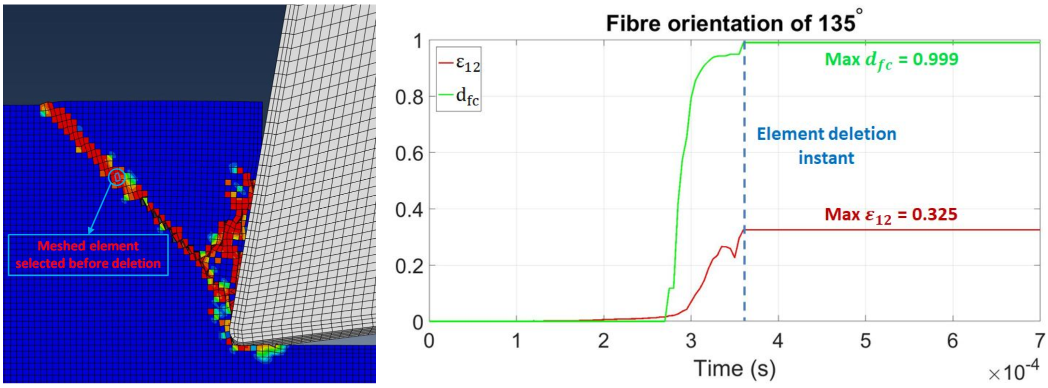

(a) (b)

Fig. 14. Representation of a representative meshed element deleted to simulate the chip of laminates with a fibre orientation of 135°: (a) Meshed element selected before deletion (b) Evolution of d_{fc} and ε_{12} during the simulation time.

4.3. Overall strain based criteria

The previous strain limit values that simulate the chip fracture in every cutting configuration studied are implemented in a VUMAT Fortran subroutine. This subroutine inserts the required features in the FE simulations to simulate the chip formation of the cases investigated in this research. Note that, because of the aim of this paper is to address a methodology to model chip formation in composite machining, the strain levels selected are determined using numerical considerations without considering an empirical basis. However, to study a particular process the measurement of maximum strains before collapse could improve significantly the accuracy in the predictions of other machining parameters such as machining forces or sub-surface damage. Finally, a high strain limit of 2 for all strain components which are not previously mentioned (ε_{11}, ε_{33}, ε_{13}, and ε_{23}) is assigned to avoid distortional problems of damaged elements. All strain limits used in this research are visualised in Table 5.

Table 5
Strain limits adopted to simulate the chip formation in all machining configurations studied

ε_{11}	$-\varepsilon_{11}$	ε_{22}	$-\varepsilon_{22}$	ε_{33}	$-\varepsilon_{33}$	ε_{12}	ε_{13}	ε_{23}
2	0.1	0.15-0.2	1.2	2	2	0.325	2	2

5. Conclusions

This paper gives a novel research on the modelling of chip formation mechanisms in composite machining. This feature is essential to simulate a machining process and its implementation to the oncoming FE studies reliably. Additionally, this work offers an effective and feasible methodology for the implementation of the chip formation in the modelling of composite machining that could be applied to study more complex machining operations such as drilling, milling or edge trimming. Five machining configurations with fibre orientations of 0°, 0° and rake angle of 0°, 45°, 90° and 135° have been successfully modelled to cover various of the most common machining scenarios. A 3D energy-based composite damage model based on the continuum damage mechanics (CDM) theory is implemented here to increase the deformation of the damaged elements and facilitate their posterior deletion. After composite laminate elements are damaged, they are selectively eroded from the simulation using a specific strain limit criterion for every simulated case to mimic the chip shape obtained in real machining processes. Main conclusions extracted from the simulations carried out in this investigation are collected in the below bullet points.

- **Fibre orientation of 0°:** The layer debonding to generate the characteristic cantilever beam effect in this chip mechanism is simulated because of the high matrix traction damage increase the transversal strains of the damaged elements abruptly. These elements are deleted in this research after their transversal strain overcomes values of 0.15. The simulation of the fibre fracture which generate the chip release need to be addressed in further investigations.

- **Fibre orientation of 0° with 0° rake angle:** Fibre micro-buckling is successfully simulated obtaining high damage fibre compression damage levels. This achievement is reached with the implementation of a compressive longitudinal strain limit of 0.1. High damage levels are observed in the laminate as a consequence of the abrupt contact of the rake face of the cutting tool with the laminate and the high contact rigidity existent for this fibre orientation.

- **Fibre orientation of 45°:** This chip is obtained because of the high shear strain levels, 0.325 or superior, obtained in the crack path. As a result, high fibre and matrix damage levels are obtained in this particular case. A small deviation of 2° of the crack path is simulated in comparison with the experimental findings. This fact occurs because of the limitations provided by the deletion of element technique employed to track the crack path accurately.

- **Fibre orientation of 90°:** Two fracture modes are modelled here in front and below of the cutting tool. In front of the tool, small chip fragments are modelled deleting the elements with high matrix compression damage and a transversal compressive strain limit of 1.2. Below the cutting tool, the fibre bending is simulated eroding the elements with high matrix tensile damage which reach tensile transversal strains of 0.2 or higher.

- **Fibre orientation of 135°:** The chip release is generated because of the high shear strains reached in this case. This is motivated for the high fibre compression damage registered in the crack area. The fibre compression Hashin's failure criterion is modified to add the shear contributions. This is achieved with the use of a new quadratic formulation and multiplying the quadratic terms associated to the shear components by a factor of 0.8.

Acknowledgements

This paper is funded by the the Engineering and Physical Sciences Research Council (EPSRC) with the grant EP/L016257/1.

References

[1] R. Nelson, C. Composites, and T. Oclv, “Bike frame races carbon consumer goods forward,” *Reinforced Plastics*, vol. 47, no. 7, pp. 36–40, 2003.

[2] Mike and P. Brady, “Technology developments in automotive composites,” *Reinforced Plastics*, vol. 54, no. 6, pp. 25–29, 2010.

[3] J. Fraga, “Boeing 787 from the Ground Up,” *AERO Magazine*, pp. 17–23, 2006.

[4] Aerospace Technology Institute (ATI), “Grow capability in complex multi-functional structures.”

[5] R. M. Saoubi, D. Axinte, S. Leung, C. Nobel, H. Attia, G. Kappmeyer, S. Engin, and W.-m. Sim, “Manufacturing Technology High performance cutting of advanced aerospace alloys and composite materials,” *CIRP Annals - Manufacturing Technology*, vol. 64, no. 2, pp. 557–580, 2015.

[6] X. M. Wang and L. C. Zhang, “An experimental investigation into the orthogonal cutting of unidirectional fibre reinforced plastics,” *International Journal of Machine Tools and Manufacture*, vol. 43, no. 10, pp. 1015–1022, 2003.

[7] V. A. Phadnis, A. Roy, and V. V. Silberschmidt, “A finite element model of ultrasonically assisted drilling in carbon/epoxy composites,” *14th CIRP Conference on Modeling of Machining Operations (CIRP CMMO)*, vol. 8, pp. 141–146, 2013.

[8] E. Persson, I. Eriksson, and L. Zackrisson, “Effects of hole machining defects on strength and fatigue life of composite laminates,” *Composites Part A: Applied Science and Manufacturing*, vol. 28, no. 2, pp. 141–151, 1997.

[9] J. L. Curiel-sosa, B. Tafazzolimoghaddam, and C. Zhang, “Modelling fracture and delamination in composite laminates : Energy release rate and interface stress,” *Composite Structures*, vol. 189, no. January, pp. 641–647, 2018.

[10] J. L. Curiel Sosa and N. Karapurath, “Delamination modelling of GLARE using the extended finite element method,” *Composites Science and Technology*, vol. 72, no. 7, pp. 788–791, 2012.

[11] N. A. Abdullah, J. L. Curiel-Sosa, Z. A. Taylor, B. Tafazzolimoghaddam, J. L. Martinez Vicente, and C. Zhang, “Transversal crack and delamination of laminates using XFEM,” *Composite Structures*, vol. 173, pp. 78–85, 2017.

[12] C. Santiuste, X. Soldani, and M. H. Miguélez, “Machining FEM model of long fiber composites for aeronautical components,” *Composite Structures*, vol. 92, no. 3, pp. 691–698, 2010.

[13] X. Soldani, C. Santiuste, A. Muñoz-Sánchez, and M. H. Miguélez, “Influence of tool geometry and numerical parameters when modeling orthogonal cutting of LFRP composites,” *Composites Part A: Applied Science and Manufacturing*, vol. 42, no. 9, pp. 1205–1216, 2011.

[14] S. Zenia, L. Ben Ayed, M. Nouari, and A. Delamézière, “Numerical analysis of the interaction between the cutting forces, induced cutting damage, and machining parameters of CFRP composites,” *International Journal of Advanced Manufacturing Technology*, vol. 78, no. 1-4, pp. 465–480, 2015.

[15] D. Wang, X. He, Z. Xu, W. Jiao, F. Yang, L. Jiang, L. Li, W. Liu, and R. Wang, “Study on Damage Evaluation and Machinability of UD-CFRP for the Orthogonal Cutting Operation Element Method,” *Materials*, vol. 10, pp. 204–224, 2017.

[16] F. Cepero-Mejías, J. L. Curiel-sosa, C. Zhang, and V. A. Phadnis, “Effect of cutter geometry on machining induced damage in orthogonal cutting of UD polymer composites : FE study,” *Composite Structures*, vol. 214, no. February, pp. 439–450, 2019.

[17] F. Cepero-Mejías, J. Curiel-Sosa, A. Blázquez, T. Yu, K. Kerrigan, and V. Phadnis, “Review of recent developments and induced damage assessment in the modelling of the machining of long fibre reinforced polymer composites,” *Composite Structures*, vol. 240, no. February, p. 112006, 2020.

[18] L. Lasri, M. Nouari, and M. El Mansori, "Modelling of chip separation in machining unidirectional FRP composites by stiffness degradation concept," *Composites Science and Technology*, vol. 69, no. 5, pp. 684–692, 2009.

[19] F. Cepero-Mejías, J. Curiel-Sosa, K. Kerrigan, and V. Phadnis, "Chip formation in machining of unidirectional carbon fibre reinforced polymer laminates: FEM based assessment," *Procedia CIRP*, vol. 85, pp. 302–307, 2019.

[20] A. Mondelin, B. Furet, and J. Rech, "Characterisation of friction properties between a laminated carbon fibres reinforced polymer and a monocrystalline diamond under dry or lubricated conditions," *Tribology International*, vol. 43, no. 9, pp. 1665–1673, 2010.

[21] G. Chardon, O. Klinkova, J. Rech, S. Drapier, and J. M. Bergheau, "Characterization of friction properties at the work material/cutting tool interface during the machining of randomly structured carbon fibers reinforced polymer with Poly Crystalline Diamond tool under dry conditions," *Tribology International*, vol. 81, pp. 300–308, 2015.

[22] Z. Hashin, "Failure Criteria for Unidirectional FibreComposites," *Journal of Applied Mechanics*, vol. 47, no. June, pp. 329–334, 1980.

[23] F. Cepero-Mejías, V. A. Phadnis, and J. L. Curiel-sosa, "Machining induced damage in orthogonal cutting of UD composites : FEA based assessment of Hashin and Puck criteria," *17th CIRP Conference on Modelling of Machining Operations*, vol. 82, pp. 332–337, 2019.

[24] A. Puck and H. Schurmann, "Failure Analysis of Frp Laminates By Means of Physically Based Phenomenological Models *," *Composites Science and Technology*, vol. 3538, no. 96, pp. 1633–1662, 1998.

[25] M. J. Hinton, A. S. Kaddour, and P. D. Soden, "A comparison of the predictive capabilities of current failure theories for composite laminates , judged against experimental evidence," *Composites Science and Technology*, vol. 62, pp. 1725–1797, 2002.

[26] F. Guo-dong, L. Jun, and W. Bao-lai, "Progressive damage and nonlinear analysis of 3D four-directional braided composites under unidirectional tension," *Composite Structures*, vol. 89, no. 1, pp. 126–133, 2009.

[27] D. H. Wang, M. Ramulu, and D. Arola, "Orthogonal cutting mechanisms of graphite/epoxy composite. Part I: unidirectional laminate," *Int. J. Mach. Tools Manufact.*, vol. 35, no. 12, pp. 1623–1638, 1995.

[28] H. Li, X. Qin, G. He, Y. Jin, D. Sun, and M. Price, "Investigation of chip formation and fracture toughness in orthogonal cutting of UD-CFRP," *The International Journal of Advanced Manufacturing Technology*, vol. 82, pp. 1079–1088, feb 2016.